buildings

MDPI

Article

Hysteresis Performance and Restoring-Force Model of Precast Concrete Ring-Lap Beam-Column Joints

Min Zhang [1,2], Zhengrong Xue [1,2], Yihu Chen [2,3,*], Dan Lu [4], Wen Qin [1,2] and Wei Yu [1,2]

[1] Key Laboratory of Green Building and Energy Efficiency, Guilin University of Technology, Guilin 541004, China
[2] College of Civil Engineering and Architectural, Guilin University of Technology, Guilin 541004, China
[3] College of Architecture and Electrical Engineering, Hezhou University, Hezhou 542899, China
[4] East China Architectural Design & Research Institute Co., Ltd., Shanghai 200002, China
* Correspondence: yihu.chen@outlook.com

Abstract: In order to study the restoring-force characteristics of precast concrete ring-lap beam-column joints, three precast concrete ring-lap beam-column joint specimens and one cast-in-place concrete beam-column joint specimen were designed and fabricated, and low-circumferential repeated loading tests were conducted. The results show that the bearing capacity of the ring-lap beam-column joint is higher than that of the cast-in-place beam-column joint, and with the increase in the lap length, the bearing capacity, ductility, and energy dissipation capacity of the ring-lap beam-column joint increase significantly, and the local damage is also mitigated. Based on the test results and the existing restoring-force model theory, a trifold restoring-force model is proposed for precast concrete ring-lap beam-column joints considering the effect of lap length. The proposed restoring-force model is consistent with the hysteresis curve of the assembled column, which indicates that the proposed restoring-force model can better reflect the influence of the lap length on the hysteresis characteristics, and can provide a reference for the structural elastic–plastic analysis and engineering application of the precast concrete ring-lap beam-column joint. The proposed restoring-force model can better reflect the influence of lap length on the hysteretic properties, which can provide a reference for the structural elastoplastic analysis and engineering application of this precast concrete ring-lap beam-column joint.

Keywords: precast concrete structures; beam-column joint; ring-lap joints; SCOPE system; restoring-force models

check for updates

Citation: Zhang, M.; Xue, Z.; Chen, Y.; Lu, D.; Qin, W.; Yu, W. Hysteresis Performance and Restoring-Force Model of Precast Concrete Ring-Lap Beam-Column Joints. *Buildings* **2023**, *13*, 286. https://doi.org/10.3390/buildings13020286

Academic Editor: Nerio Tullini

Received: 2 December 2022
Revised: 6 January 2023
Accepted: 11 January 2023
Published: 18 January 2023

Copyright: © 2023 by the authors. Licensee MDPI, Basel, Switzerland. This article is an open access article distributed under the terms and conditions of the Creative Commons Attribution (CC BY) license (https://creativecommons.org/licenses/by/4.0/).

1. Introduction

Reinforced concrete (RC) components have been widely used in the design of both civilian and military protective structures, especially beam-column joints. The reliability of precast beam-column joints has a significant effect on structural integrity and seismic performance and plays a crucial role in the structure's connections [1–4]. The traditional prefabricated beam-column joint connection is made by extending the lower reinforcement of the prefabricated beam into the prefabricated column for the lap joint and pouring concrete afterward, as shown in Figure 1. Since the steel bars of precast beams are anchored into the joints inside the columns, the joints have dense steel bars in the core area, which makes the process of concrete placement difficult, and the construction process complicated and inefficient. In the 1980s, domestic and foreign researchers began to extensively study a frame structure composed of a secant system [5–9], which forms a continuous load transfer system by placing open-type bent-anchored reinforcement in the precast columns, lapping with the L-shaped reinforcement protruding from the bottom of the beam ends, and post-casting concrete, as shown in Figure 2. This frame structure places the lap joint area at the beam end, avoiding the beam-column joint and improving the difficult problem of dense reinforcement within the beam-column joint. However, the connection requires a long lap

length, resulting in a long post-cast area at the beam end. Many of the studies showed that the interface between the U-shape steel reinforcement and the concrete was the weakest link of the connection, and damage in the bottom of the key slot end often resulted in the final failure of the specimen [10,11]. For this reason, it is necessary to ensure that there is sufficient lap length between the U-shaped steel bars and protruding bottom reinforcement of the precast beam. Therefore, this paper proposes a new type of precast concrete ring-lap beam-column joint, as shown in Figure 3, in which the steel bars protruding from the bottom of the beam ends are bent 180° to form a bend hook and lap with the closed-loop bars placed in the prefabricated column, to enhance the anchorage capacity and shorten the length of the post-cast area at the beam end.

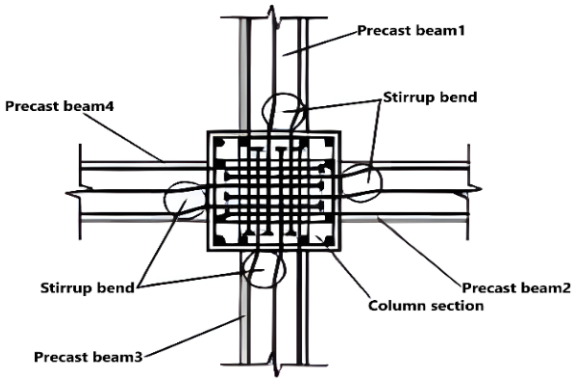


Figure 1. Traditional prefabricated beam-column joint.

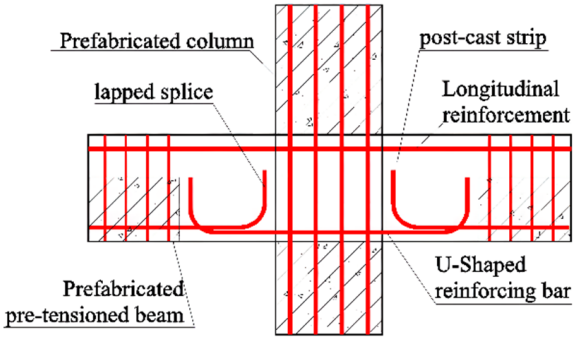


Figure 2. SCOPE system.

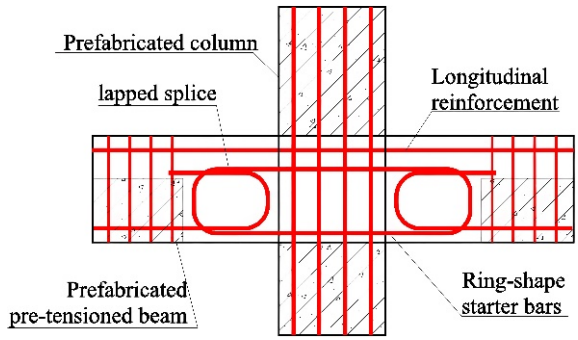


Figure 3. Ring buckle lap beam-column joint.

At this stage, domestic and foreign researchers tend to study the hysteresis characteristics and restoring-force models of members through low-circumferential reciprocal loading tests. H. Rodrigues et al. [12] analyzed the biaxial cyclic behavior of reinforced concrete columns using a trifold-type restoring-force model. Yan Changwang et al. [13] developed a trifold linear restoring-force model for the hysteretic properties of steel-bone ultra-high strength concrete frame joints, and Guifeng Z. et al. [14] also used a trifold linear

restoring-force model to analyze the hysteretic properties of corroded reinforced concrete frame columns. The keyway beam bottom bar anchored into a precast beam-column connection studied by Guan Dongzhi et al. used a flat-top trifold-type skeleton curve to establish the restoring-force model [15]. Xue Jianyang et al. [16] conducted a proposed static force test for the beam-column joints of concrete antique buildings with attached viscous dampers and obtained the fourfold linear restoring-force model of the joints by fitting. Ding Wei et al. [17] sought rules from the skeleton curves of composite-shear walls with concealed bracings in steel-tube frames (composite-shear walls), and thereby developed the quadric-linear restoring-force model in this study. While the curvilinear restoring-force model can simulate the test results well, it has not been widely used due to the relative complexity of the calculation [18]. Combined with the above research by domestic and foreign scholars, it is found that the trifold model is more suitable for the application of the restoring-force model of beam-column joints. In addition, for the conventional beam-column joints, the trifold model has better applicability; however, for the hysteresis curves with the obvious pinching phenomenon, the symmetric trifold hysteresis rule can be better used to obtain the restoring-force model [19,20].

In this paper, one cast-in-place beam-column joint with three precast concrete ring-lap beam-column joints was fabricated according to the lap length of assembled concrete beam-column ring-buckle-lap joints, and low-circumferential cyclic loading tests were conducted. By comparing and analyzing the hysteresis curves and skeleton curves of the tests, a trifold restoring-force model applicable to the beam-column joint with ring-lap was proposed, and a symmetric trifold hysteresis rule conforming to this connection was obtained by using linear fitting. The restoring-force model is compared with the experimental results to provide a theoretical basis for the engineering application of this new beam-column joint.

2. Form of Construction

2.1. Introduction to the Loop Fastening Technique

The new ring-buckle connection technology proposed in this paper is to use U-shaped load-bearing reinforcement at the bottom of the prefabricated beam end at the beam-column joint, and ring-shaped reinforcement at the column joint as the beam-column connection reinforcement, with the upper reinforcement and the cast-in-place part unchanged, and to put four short bars through the four corners of the lap ring-buckle area and encrypt the hoops in the connection section of the ring-buckle site, with the connection schematic shown in Figure 4. The load-carrying mechanism forms a continuous load transfer system; the steel bars protruding from the bottom of the beam ends are bent 180° to form a bend hook, and lap with the closed-loop bars placed in the prefabricated column from the bottom of the beam ends, and the connection is completed with post-casting concrete.

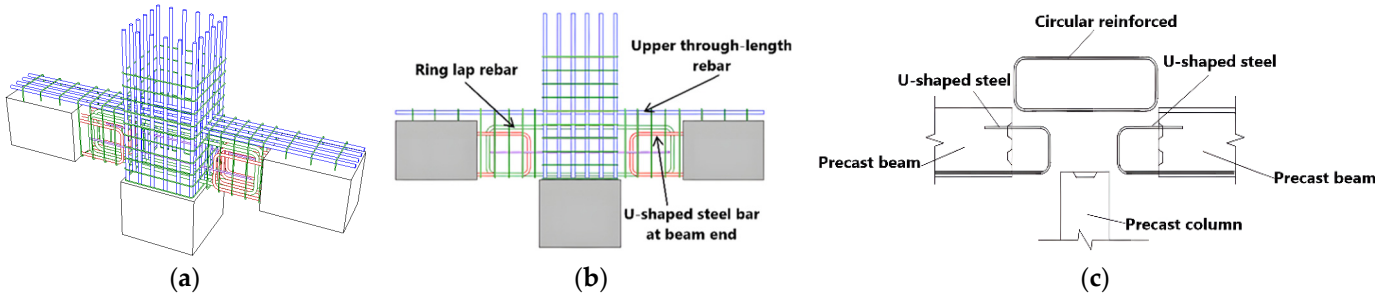


Figure 4. Schematic diagram of ring-buckle connection: (**a**) 3D view of the beam-column connection; (**b**) Front view of the beam-column connection; (**c**) Schematic diagram of ring reinforcement drawdown.

2.2. Test Piece Design

One conventional cast-in-place beam-column joint specimen and three ring-lap beam-column joint specimens, numbered XJ-1, UX-1, UX-2, and UX-3, were designed and produced, in which the longitudinal reinforcement and hoop reinforcement in the columns

were identical. The beams were symmetrically reinforced, and the reinforcement rates of all members were the same except for the different construction forms. Cast-in-place beam-column joint specimen XJ-1 and ring-lap joint specimen UX-1, specimen UX-2, specimen UX-3 showed the structural form of the specimens as shown in Figure 5 and the design parameters of each specimen as shown in Table 1. The concrete strength grade of the specimens is C30. The mechanical properties of the concrete specimens were tested according to the Standard for Mechanical Properties of Ordinary Concrete (GB50081-2002) [21], and the test results are shown in Table 2. By the test method of "Tensile test for metallic materials Part 1: Room temperature test method" (GB/T228.1-2010) [22], the mechanical material tensile test was carried out on steel bars, and the test results are shown in Table 3.

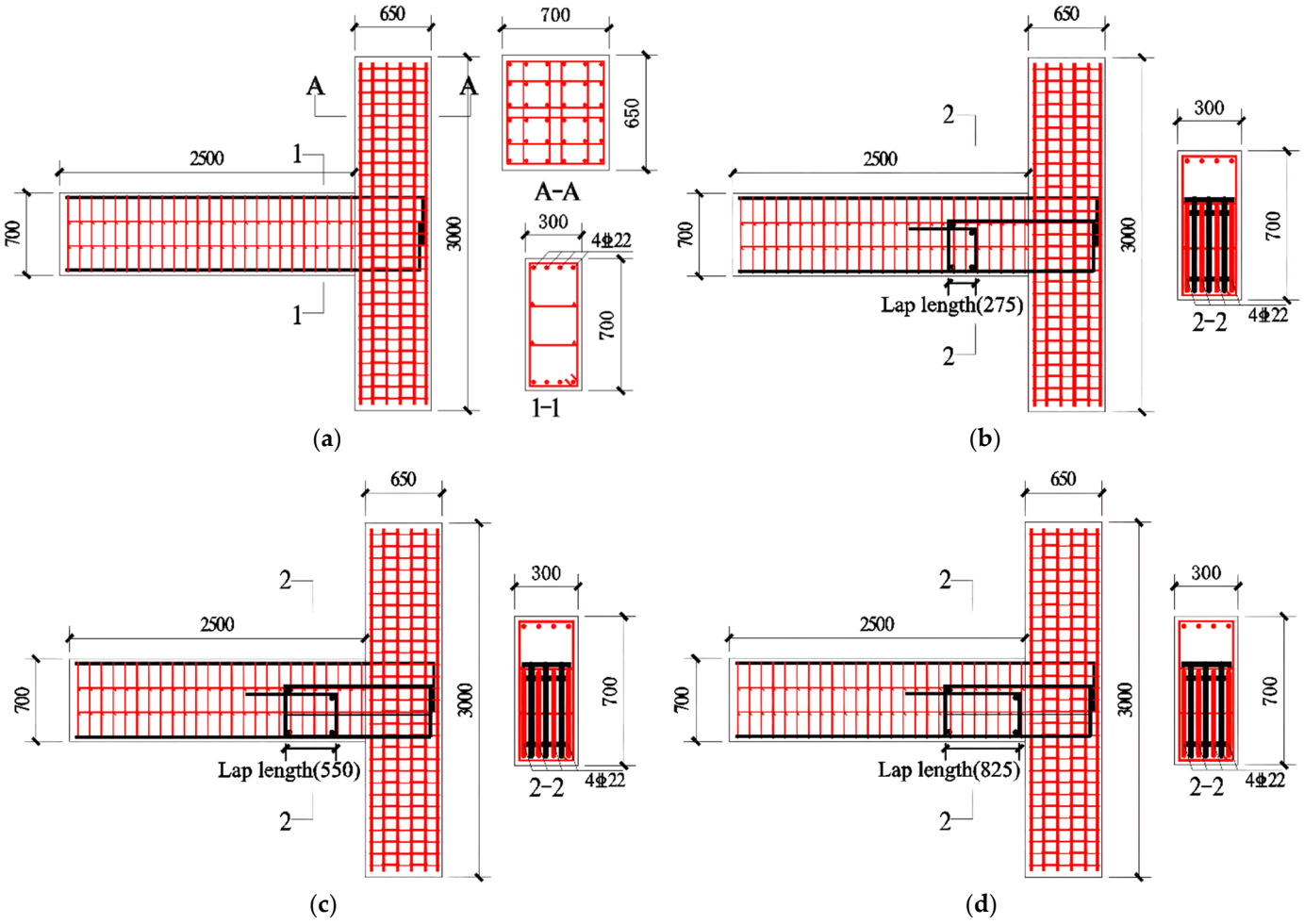


Figure 5. Constructional form of the specimen: (**a**) Specimen XJ-1; (**b**) Specimen UX-1; (**c**) Specimen UX-2; (**d**) Specimen UX-3.

2.3. Test Piece Production

For the cast-in-place beam-column joint specimen XJ-1, the reinforcement cage was tied following the reinforcement allocation and then poured. For ring-lap beam-column joint specimens UX-1, UX-2, and UX-3, all were cast in the form of a secondary concrete pour, first placing a rigid spacer at the joint position, followed by pouring the foundation column and the part of the beam beyond the joint, then removing the wooden spacer after it had hardened, and then pouring the concrete in the joint area. The purpose of the secondary pour was to simulate the assembly construction process. Finally, the specimens were cured for 28 days and were then ready for testing. Figure 6 shows the fabrication process and the completed elements.

Table 1. Specimen design parameters.

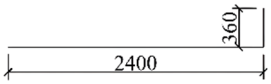
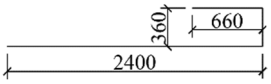
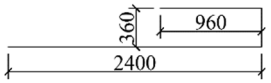
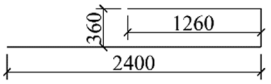
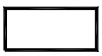
Number	Connection Joints	Form of Longitudinal Reinforcement	Longitudinal Reinforcement	Form of Lap Reinforcement	Lap Reinforcement	Lap Length
XJ-1	Cast-in-place junction		4C22	—	—	—
UX-1	Ring lap joints		4C22		3C25	275
UX-2	Ring lap joints		4C22		3C25	550
UX-3	Ring lap joints		4C22		3C25	825

Table 2. Mechanical properties of concrete materials.

f_{cu}/MPa	$\overline{f_{cu}}$/MPa	f_{cu}/MPa	$\overline{f_{cu}}$/MPa	*E*/MPa
36.4	32.65	23.6	24.85	3.0×10^4
35.2		22.5		
32.5		24.8		
29.4		27.6		
30.6		29.1		
31.8		21.5		

Table 3. Mechanical properties of reinforcing steel materials.

Type of Reinforcement	Reinforcement Grades	Diameter /mm	$\overline{f_y}$/Mpa	$\overline{f_u}$/Mpa
Longitudinal reinforcement	HRB400	22	402.8	606.9
		25	405.6	609.3
Hoop reinforcement		8	402.1	605.9
		8	402.1	605.9



(**a**)



(**b**)



(**c**)

Figure 6. Fabrication and completion of the test piece: (**a**) Tying of reinforcement cage; (**b**) Second casting; (**c**) Completion of casting.

2.4. Loading Options

According to the relevant codes of the Seismic Test Procedure for Buildings (JGJ/T101-2015) [23], this test was carried out by applying horizontal proposed static loading at the cantilevered end of the beam, fixing the column body to the ground and applying horizontal pressure by jacks at both ends to ensure that the column body would not follow the horizontal movement of the beam ends during the loading process. Figure 7 shows the test loading site. To simulate the effect of repeated loading, cyclic loading Δ/Lbeam = 0.2%, 0.4%, 0.8%, 1.2%,

1.6%, 2%, 2.4%, 2.8%, 3.2%, and 3.6% was carried out according to the angular amplitude of floor displacement, with three cycles for each amplitude. The maximum floor displacement angle of 3.6% tested in the experiments far exceeded the allowable elastoplastic limits specified in the Code for Seismic Design of Buildings (GB50011-2010) [24] to simulate severe earthquake damage. The loading was terminated when the specified maximum displacement was reached, or the horizontal load was reduced to 85% of the maximum value. Figure 8 shows a graph of the test loading curve.

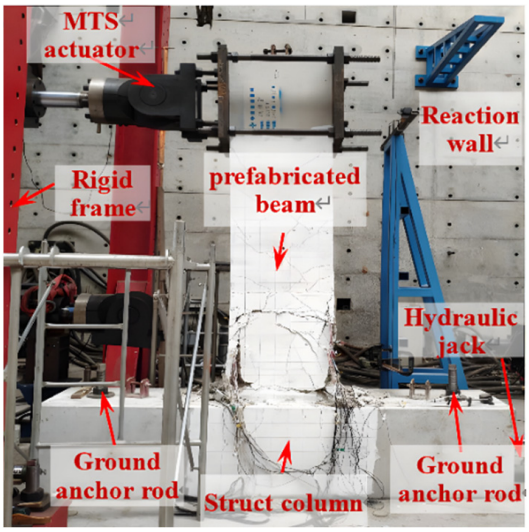


Figure 7. Test loading site.

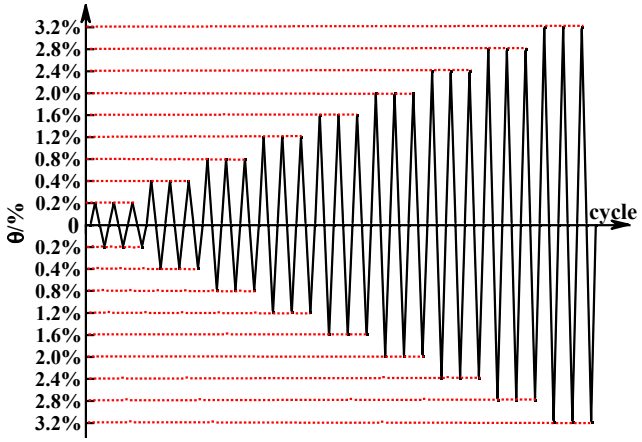


Figure 8. Test loading curve.

3. Test Curve Analysis and Skeleton Curve Modeling

3.1. Hysteresis Curve Analysis

The hysteresis curve is the load-displacement curve of the member under the action of the proposed static force, reflecting the energy dissipation capacity of the joint and the trend of the bearing capacity. The hysteresis curve for each specimen, derived through the proposed static force low-circumferential reciprocal test, is shown in Figure 9. It can be seen that the existing specimen XJ-1 hysteresis curve is relatively complete, the hysteresis loop presents a typical shuttle shape, and the forward loading and reverse loading hysteresis curve presents a symmetrical distribution. Before displacement exceeds 0.4%, the loading force curve of the specimen shows a linear distribution, then the load increase is minimal, and the displacement increases; at around 2.8% of displacement, the horizontal load of the specimen reaches its peak, and then the load decreased. The hysteresis curve did not show any apparent pinching phenomenon.

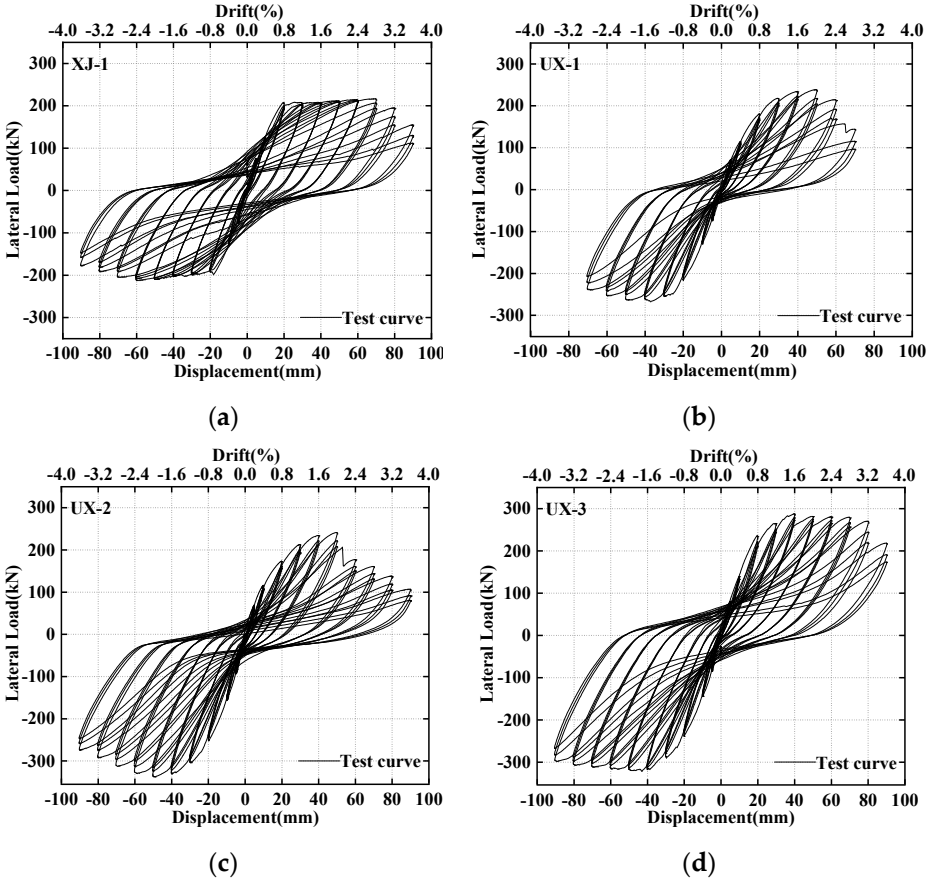


Figure 9. Hysteresis curve for each specimen: (**a**) Specimen XJ-1; (**b**) Specimen UX-1; (**c**) Specimen UX-2; (**d**) Specimen UX-3.

The hysteresis curve of specimen UX-1 shows that the curve is generally symmetrical overall. When the displacement is within the range of 0.4%, the loading curve of the specimen is linearly distributed; when the removal of positive and negative loading is about 2%, the specimen reaches the bearing capacity, after which the load gradually decreases with the increase in displacement.

The hysteresis curve of specimen UX-2 is asymmetrical and has the phenomenon of "pinching" compared to specimen A. When the displacement amount is lower than 0.4%, the loading force curve of the specimen is linearly distributed; after that, the change of the forward and reverse loading curves is different; when the displacement amount of reverse loading reaches 2%, the specimen reaches the peak bearing capacity, and after that the load decreases slightly with the increase in the displacement amount; when the displacement amount of forward loading reaches 2%, the specimen reaches the peak bearing capacity. However, the corresponding value is smaller than that of the reverse loading, after which the load decreases faster as the displacement increases.

The hysteresis curve of specimen UX-3 has good symmetry and a certain degree of "pinching" phenomenon. In the elastic phase, i.e., at the beginning of loading, the curve is linear, with very little energy dissipation in the member. After this, it increases gradually and changes non-linearly. When the displacement of the load reaches 2%, the specimen also reaches the peak load capacity, and then the load starts to decrease gradually until it falls below 85% of the peak load.

Comparing the hysteresis curves for the four specimens under low-circumferential reciprocating loads, the following conclusions can be drawn:

The peak load of beam-column joint specimens UX-1, UX-2, and UX-3 with loop lap joints is higher than that of cast-in-place beam-column joint specimen XJ-1. Still, the hysteresis curve has the phenomenon of "pinching," which indicates that the skeleton in

the connection area shows slippage. Comparing three specimens of beam-column joints with ring-buckle and lap, it can be found that with the increase in the lap length, the load capacity of the specimen is increased, and the "pinching" phenomenon is relatively reduced, which indicates that the increase in the lap length can help to reduce the degree of reinforcement slippage. In addition, as the lap length increases, the rate of reduction in load-carrying capacity decreases, indicating that the increase in lap length helps to mitigate local damage to the concrete.

The above hysteresis curve analysis shows that the seismic performance of ring-lap beam-column joints is better than that of cast-in-place beam-column joints, so it is of practical significance to study the restoring-force model of ring-lap beam-column joints.

3.2. Skeleton Curve Analysis

The skeleton curve is an essential basis for determining the characteristic points in the restoring-force model by presenting the maximum load value for the first cycle of each level of loading displacement in the hysteresis curve, forming a new trajectory curve. The characteristic point of the skeleton curve is an essential factor in reflecting the curve's trend, which can be derived from the displacement corresponding to the yield load of the member, the displacement corresponding to the maximum load, and the displacement corresponding to the ultimate load, etc. The skeleton curves of the three loop lap members are shown in Figure 10, from which it can be found that the skeleton curves of the loop lap members can be roughly divided into the following three stages of the changing trend.

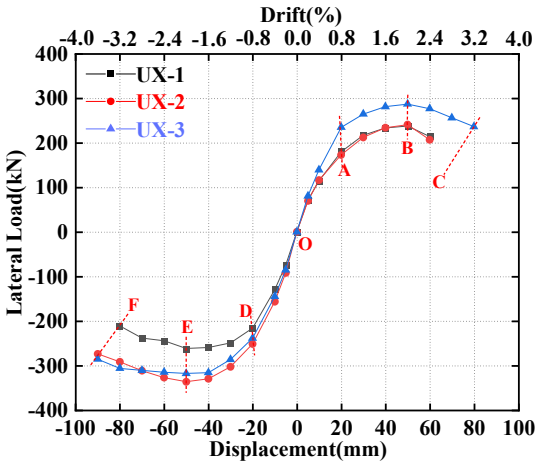


Figure 10. Skeleton curve for each specimen.

The slope of the OA and OD sections indicates the elastic stiffness of the member, and the load rises significantly with the displacement increase, showing a linear relationship, which represents the force characteristics of the member in the elastic phase.

The slope of the AB/DE section indicates the stiffness of the member; with the increase in displacement, the load rises more slowly than the OA/OD section, probably due to the degradation of stiffness, the increase in concrete cracks, and the reduction in reinforcement strength. This may be due to stiffness degradation, increased concrete cracking, and reduced reinforcement strength.

The slope of the BC and EF sections indicates the softening stiffness of the member, after which the load decreases with increasing displacement, the stiffness degrades more significantly, the reinforcement yields, and the member eventually loses its load-carrying capacity. The force characteristics are consistent with the macroscopic damage state of the member.

By observing the skeleton curves of the three ring-lap beam-column joint members, it is found that the general trend of change follows the three stages described above, which reflect the force condition of the members more intuitively.

3.3. Proposed Skeleton Curve Model

The skeleton curve obtained from the test results can be roughly divided into the above three stages. As different members develop damage to varying joints during the stressing process, it is impossible to see exactly how each stage changes, and using a unified formula for expression is impossible. Therefore, the skeleton curves obtained from the test results need to be dimensionlessly processed by taking the ratio of the load P corresponding to each stage of displacement to the maximum load Pm throughout the test process (P/P_m) and the ratio of the removal Δ at each location to the expulsion Δ_m corresponding to the maximum load (Δ/Δ_m) to obtain the corresponding P/P_m~Δ/Δ_m skeleton curves, as shown in Figure 11.

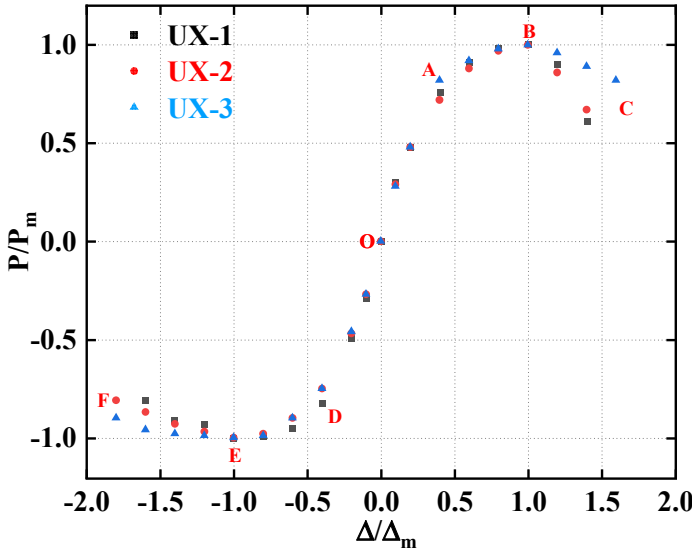


Figure 11. Dimensionless skeleton curve.

By observing the skeleton curves of the dimensionless treatment, it can be found that the skeleton curves of the three different lap lengths show a similar trend; only in the degradation stage, due to the apparent difference in the stiffness degradation of various members leading to an inevitable variability of the curves, the elastic step, and the yielding stage match. Therefore, the dimensionless skeleton curve can be expressed as a trifold skeleton curve model.

The trifold skeleton curve model obtained after linear regression fitting is shown in Figure 12. Point A (0.4, 0.8) in the figure is the yield point for favorable loading, and point D (−0.4, −0.8) is the yield point for negative loading. The tangent method determines the yield point [25] and is then verified by the equivalent elastic–plastic yielding method [26]. Point B (1, 1) is the displacement point corresponding to the maximum load that the member can withstand during favorable loading, and point E (−1, −1) is the displacement point corresponding to the maximum load that the member can withstand during negative loading, which can be obtained simply by statistical observation. Points C (1.6, 0.7) and F (−1.6, −0.8) are the damage points corresponding to positive and negative loading, i.e., determined by dropping the load to below 85% of the ultimate load. The regression equations and slopes for each stage are shown in Table 4.

3.4. Comparison of Skeleton Curve Model and Experimental Skeleton Curve

The regression equations for each stage obtained from Table 3 were substituted into the skeleton curves of the beam-column joints for the three lap lengths. Taking UX-1 as an example, P_m^+ = 237.83 kN and Δ_m^+ = 50 mm were substituted into the regression equation for the OA section to obtain P = 9.7777 × Δ, and so on, to receive the dimensioned skeleton curves for UX-1, UX-2, and UX-3. The calculated dimensional skeleton curves were compared with the test results of the three components, respectively, as shown in

Figure 13. The comparison shows that although there is some deviation between the skeleton curve model and the skeleton curves obtained from the tests, they can match. It indicates that the fitted trifold skeleton curve model better reflects the load-displacement curve relationship of the ring lap of the assembled concrete beam-column joints of the geometrical configurations and material properties used in this study.

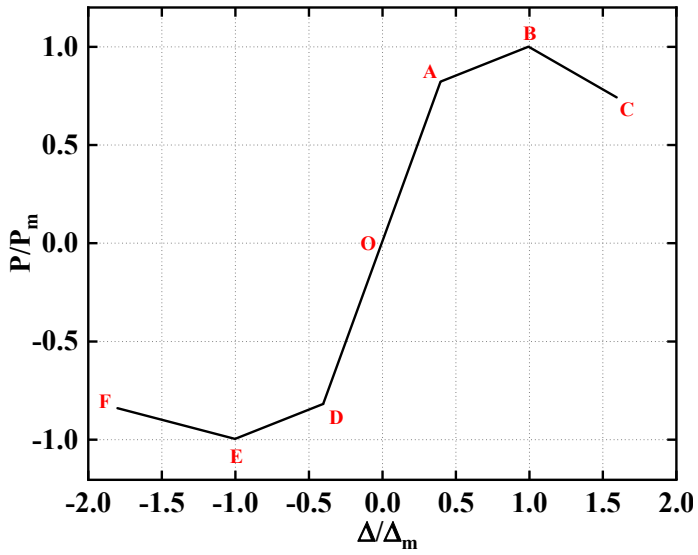


Figure 12. Skeleton curve model.

Table 4. Regression equations for each stage of the skeleton curve model.

Stage	Regression Equation	Slope
OA	$P/P_m^+ = 2.0556\Delta/\Delta_m^+$	2.0556
AB	$P/P_m^+ = 0.2963\Delta/\Delta_m^+ + 0.7037$	0.2963
BC	$P/P_m^+ = -0.4292\Delta/\Delta_m^+ + 1.4292$	−0.4292
OD	$P/P_m^+ = 2.0556\Delta/\Delta_m^+$	2.0556
DE	$P/P_m^+ = 0.2963\Delta/\Delta_m^+ - 0.7037$	0.2963
EF	$P/P_m^+ = -0.1948\Delta/\Delta_m^+ - 1.1948$	−0.1948

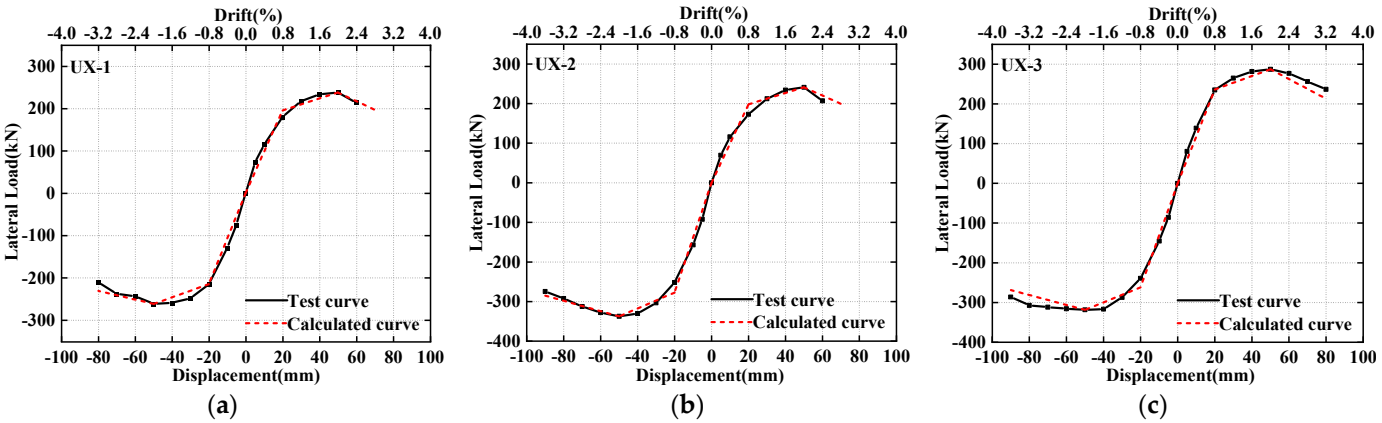


Figure 13. Comparison of skeleton curve calculation results with test results: (**a**) Specimen UX-1; (**b**) Specimen UX-2; (**c**) Specimen UX-3.

4. Restoring-Force Model

4.1. Hysteresis RULES

The loading and unloading process of the component can be described based on the above skeleton curve model and the hysteresis rules. The hysteresis rules are listed below and are shown in Figure 14.

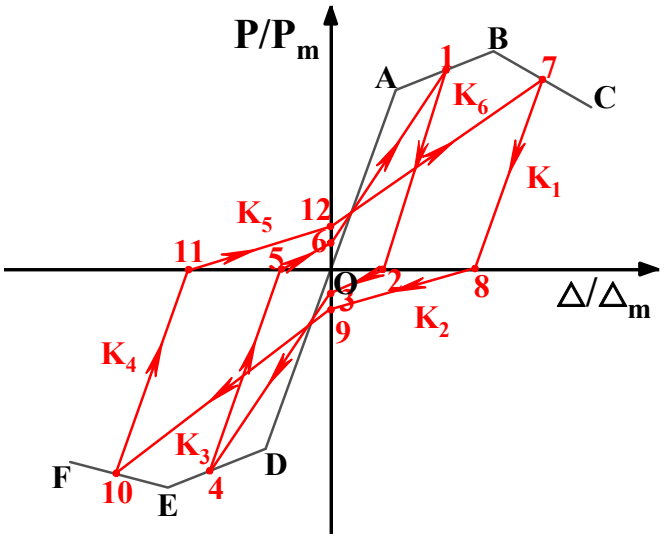


Figure 14. Hysteresis Rules.

(1) Positive loading is performed along the skeleton curve O–A–B–C, while negative loading is along O–D–E–F. Unloading along the O–A(O–D) section (elastic phase) occurs along the A–O(D–O) direction, i.e., the unloading stiffness in the flexible stage corresponds to the initial stiffness as denoted by $K_0^+(K_0^-)$.

(2) When unloading at point 1 (strengthening phase), it first unloads to point 2 with the forward unloading stiffness of K_1, then reversely loads to tell 3 with the initial reverse loading stiffness of K_2. Subsequently, reverse loading is performed along the 3–4 direction with the latter reverse loading stiffness of K_3. When unloading at point 4, it reversely unloads to 5 with the reverse unloading stiffness of K_4. Forward reloading is performed along the 5–6–1 direction with the initial and later forward loading stiffness of K_5 and K_6, respectively. This loading pattern continues in successive cycles. Therefore, the overall loading and unloading cycle follows the O–A–1–2–3–4–5–6–1–B–7 route.

(3) When unloading at point 7 (softening phase), it first unloads to point 8 with the forward unloading stiffness of K_1, then reversely loads to tell 9 with the initial reverse loading stiffness of K_2. Subsequently, reverse loading is performed along the 9–10 direction with the latter reverse loading stiffness of K_3. When unloading at point 10, it reversely unloads to 11 with the reverse unloading stiffness of K_4. Forward reloading is performed along the 11–12–7 direction with the initial and later forward loading stiffness of K_5 and K_6, respectively. This loading pattern continues in successive cycles. Therefore, the overall loading and unloading cycle follows the O–A–B–7–7–8–9–10–11–12–7–C route.

It can be observed in the experimental load-displacement curves, as shown in Figure 8, that at the same displacement control level, the unloading curves of different cycles nearly coincide. In contrast, the loading curves degrade to varying degrees. Hence, the unloading stiffness remains constant during three-cycle displacement loading. For simplicity, the loading stiffness is also considered to be the same. At different displacement control levels, however, the loading and unloading stiffness gradually decreases with the increase in the loading displacement, known as stiffness degradation. The phenomenon of stiffness degradation is caused by crack development, steel reinforcement yield, and accumulation of plastic damage in concrete. The degradation of stiffness is discussed as follows to obtain the loading and unloading stiffness.

4.2. Stiffness Degradation

As indicated by the restoring-force model, the secant stiffnesses are considered in this study to reflect the component stiffness at all phases. To analyze the relationship between the secant stiffnesses and the displacement load level, the stiffness–displacement test data are normalized as shown in Figure 15a–f. The y-axis expressed as $K_i/K_0^+(K_0^-)$

(i = 1,2, . . . ,6) corresponds to the ratios of the secant stiffnesses to the initial component stiffness, where K_1 is the forward unloading stiffness, K_2 is the initial reverse loading stiffness, K_3 is the latter reverse loading stiffness, K_4 is the reverse unloading stiffness, K_5 is the initial forward loading stiffness, and K_6 is the latter forward loading stiffness as considered in the restoring-force model. Meanwhile, the x-axis corresponds to either the loading displacement levels $\Delta_1/\Delta_m{}^+$ ($\Delta_4/\Delta_m{}^-$) or the residual displacement ratios $\Delta_2/\Delta_m{}^+$ ($\Delta_5/\Delta_m{}^-$), where $\Delta_1(\Delta_4)$ and $\Delta_2(\Delta_5)$ are the loading displacement upon unloading and residual displacement after complete unloading in the positive (negative) direction, respectively. Given the trend of the stiffness degradation, the exponential fitting equation expressed as $y = A \times e^{-B*x}$ is considered, and the equations for each stage are shown in Table 5. Figure 15a–f shows the fitted stiffness-degradation curves and associated control parameters. The coefficient of determination for curve fitting varies between 0.82 and 0.92, indicating reasonably good fits. Therefore, the stiffness-degradation curve fitting equations can be used to effectively determine the loading and unloading stiffness at phases other than the elastic phase.

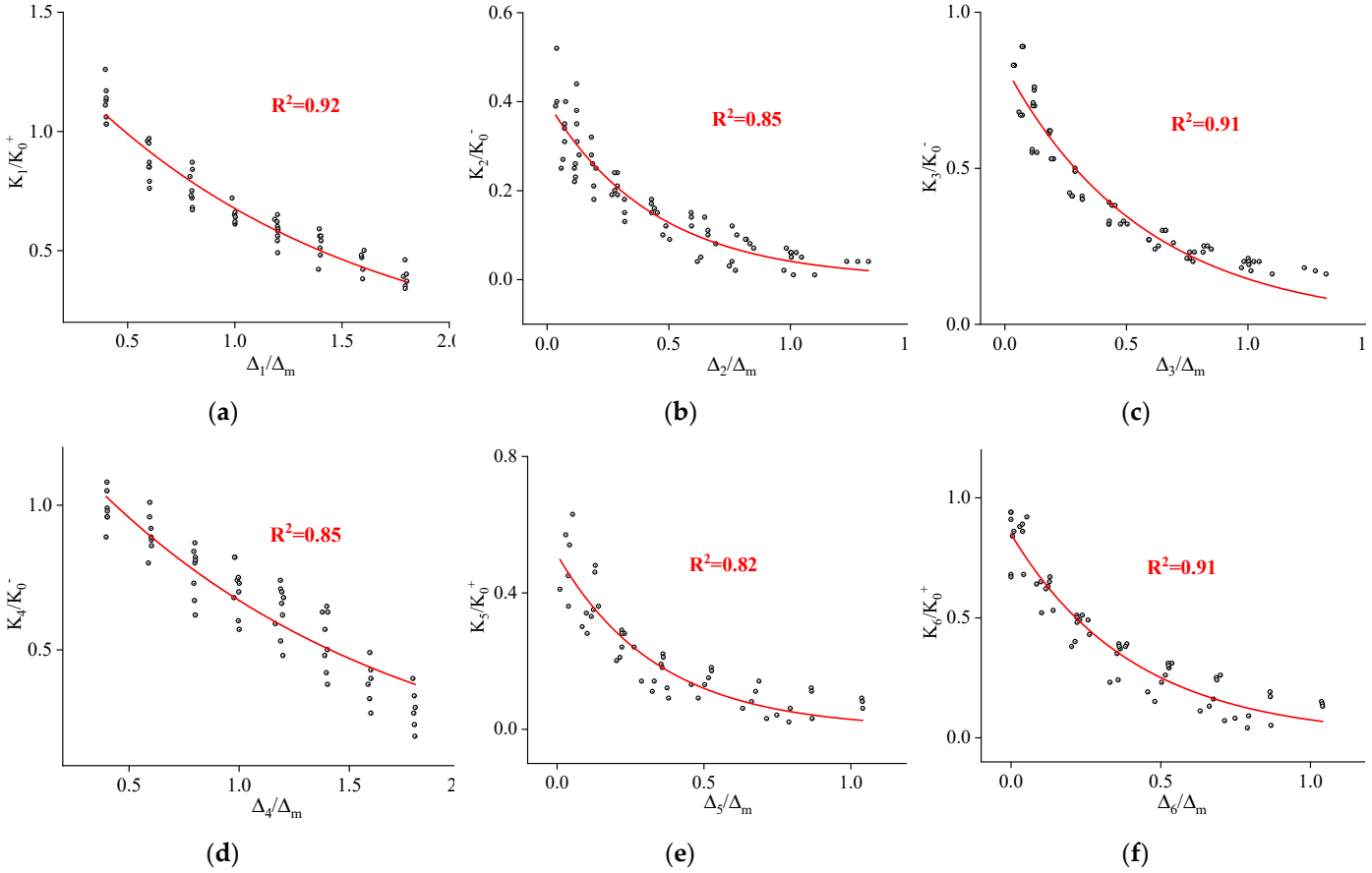


Figure 15. Regression analyses of stiffness-degradation curves: (**a**) $K_1/K_0{}^+$; (**b**) $K_2/K_0{}^-$; (**c**) $K_3/K_0{}^-$; (**d**) $K_4/K_0{}^-$; (**e**) $K_5/K_0{}^+$; (**f**) $K_6/K_0{}^+$.

Table 5. The regression equation for each degradation stage.

Stage	Regression Equation
$K_1/K_0{}^+$	$K_1/K_0{}^+ = 1.4733 \times e^{(-0.7191*\Delta 1/\Delta m+)}$
$K_2/K_0{}^-$	$K_2/K_0{}^- = 0.9156 \times e^{(-1.9001*\Delta 2/\Delta m-)}$
$K_3/K_0{}^-$	$K_3/K_0{}^- = 1.5469 \times e^{(-1.2608*\Delta 3/\Delta m-)}$
$K_4/K_0{}^-$	$K_4/K_0{}^- = 1.4207 \times e^{(-0.6684*\Delta 4/\Delta m-)}$
$K_5/K_0{}^+$	$K_5/K_0{}^+ = 1.5387 \times e^{(-1.8446*\Delta 5/\Delta m+)}$
$K_6/K_0{}^+$	$K_6/K_0{}^+ = 1.7717 \times e^{(-1.5109*\Delta 6/\Delta m+)}$

According to the basic hysteresis rules shown in Figure 14, the hysteresis curves of the ring-lapped splice joint can then be obtained. A comparison of the results obtained using the restoring-force model and test data of each specimen is depicted in Figure 16. The comparison indicates that the result obtained using the restoring-force model can be considered feasible.

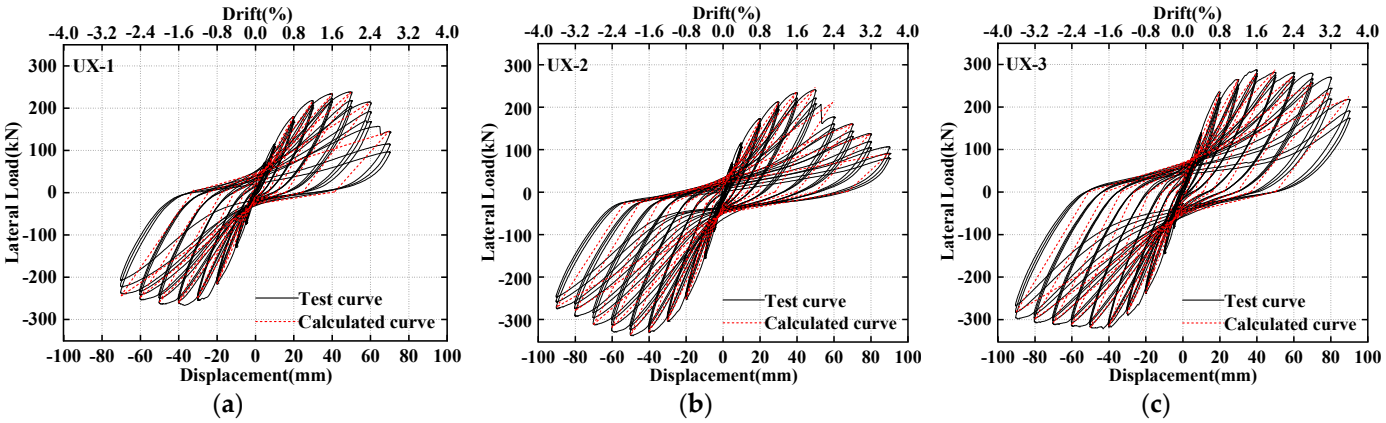


Figure 16. Comparison of hysteresis curves obtained by the restoring-force model and experiment: (**a**) Specimen UX-1; (**b**) Specimen UX-2; (**c**) Specimen UX-3.

5. Conclusions

This paper reviewed the development of the ring-lapped splice beam-column connection to improve the connection quality of precast reinforced concrete components and their cyclic performance with different lap lengths. On this basis, a restoring-force model was established based on measured load-displacement curves considering the softening or stiffness degradation. The main conclusions are as follows:

(1) According to the comparison of the hysteresis curves, it can be found that the bearing capacity of the ring-lap joint of UX-3 is significantly higher than that of the cast-in-place joint, while the bearing capacity and stiffness of the side of the beam with the lap is significantly greater than that of the other side during the reciprocal loading process.

(2) With the increase in the lap length, the bearing capacity, ductility and energy dissipation capacity of the specimen increase, and the slip of the reinforcement inside the concrete is also slowed down. Therefore, the effect of lap length on the hysteresis characteristics of the specimen should be considered when modeling the restoring-force of the precast concrete ring-lap beam-column joint.

(3) Based on the analysis of the experimental data and linear fitting, the formulae for calculating the characteristic parameters of the skeleton curve of the assembled ring-lap beam-column joints were obtained, and the comparison between the experimental and calculated results showed that they were consistent. It shows that the formula is applicable to the assembled ring-lap beam-column joints with different lap lengths.

(4) By calculating the theoretical hysteresis curves of the specimens and comparing them with the test results, it was found that they were in high agreement. This indicates that the symmetric trifold hysteresis rule established in this paper can effectively reflect the hysteresis characteristics of the precast concrete ring-lap beam-column joint with different lap lengths.

Author Contributions: M.Z., conceptualization, funding acquisition, investigation, and formal analysis; Z.X., data curation, software, writing—original draft preparation, and formal analysis; Y.C., conceptualization, project administration, supervision, and formal analysis; D.L., methodology, investigation, funding acquisition, and formal analysis; W.Q., data curation and formal analysis; W.Y., data curation, and formal analysis. All authors have read and agreed to the published version of the manuscript.

Funding: This research was funded by the National Natural Science Foundation of China (No. 51868013) and the Guangxi Key Research Program (Guike AB22036001, Guike AB21220046).

Institutional Review Board Statement: Not applicable.

Informed Consent Statement: Not applicable.

Data Availability Statement: The data presented in this study are available on request from the corresponding author.

Acknowledgments: We thank the National Natural Science Foundation of China (No. 51868013) and Guangxi Key Research Program (Guike AB22036001, Guike AB21220046) for their support, and the Key Laboratory of Green Building and Energy Efficiency (Guikeneng 17-J-21-9). Any views, findings, and conclusions expressed in this article do not represent the views of the Key Laboratory of Green Building and Energy Efficiency and the National Natural Science Foundation of China.

Conflicts of Interest: The authors declare no conflict of interest.

References

1. Anas, S.M.; Alam, M.; Umair, M. Experimental and numerical investigations on performance of reinforced concrete slabs under explosive-induced air-blast loading: A state-of-the-art review. *Structures* **2021**, *31*, 428–461. [CrossRef]
2. Men, J.; Fan, G.; Lan, T.; Wang, J.; Xiong, L. Study on the Seismic Performance of Box-Plate Steel Structure with Openings Modular Unit. *Materials* **2019**, *12*, 4142. [CrossRef] [PubMed]
3. Berman, J.W. Seismic behavior of code designed steel plate shear walls. *Eng. Struct.* **2011**, *33*, 230–244. [CrossRef]
4. Xue, W.; Hu, X.; Song, J. Experimental study on seismic behavior of precast concrete beam-column joints using UHPC-based connections. *Structures* **2021**, *34*, 4867–4881. [CrossRef]
5. Kurama, Y.C.; Sritharan, S.; Fleischman, R.B.; Restrepo, J.I.; Henry, R.S.; Cleland, N.M.; Ghosh, S.K.; Bonelli, P. Seismic-Resistant Precast Concrete Structures: State of the Art. *J. Struct. Eng.* **2018**, *144*, 03118001.1–03118001.18. [CrossRef]
6. Brunei, E.; Nascimbene, R.; Bolognini, D.; Bellotti, D. Experimental investigation of the cyclic response of reinforced precast concrete framed structures. *PCI J.* **2015**, *60*, 57–79. [CrossRef]
7. Yang, J.; Guo, T.; Chai, S. Experimental and numerical investigation on seismic behaviors of beam-column joints of precast prestressed concrete frame under given corrosion levels. *Structures* **2020**, *27*, 1209–1221. [CrossRef]
8. Xue, W.; Hu, X.; Ren, D.; Hu, X. Seismic behavior of precast 100 MPa grade HSC frames under reversed cyclic loading. *Eng. Struct.* **2021**, *243*, 112662. [CrossRef]
9. Choi, H.K.; Choi, Y.C.; Choi, C.S. Development and testing of precast concrete beam-to-column connections. *Eng. Struct.* **2013**, *56*, 1820–1835. [CrossRef]
10. Chen, Y.; Zhang, Q.; Feng, J.; Zhang, Z. Experimental Study on Shear Resistance of Precast RC Shear Walls with Novel Bundled Connections. *J. Earthq. Tsunami* **2019**, *13*, 661–672. [CrossRef]
11. Ameli, M.J.; Pantelides, C.P. Seismic analysis of precast concrete bridge columns connected with grouted splice sleeve connectors. *J. Struct. Eng.* **2017**, *143*, 04016176. [CrossRef]
12. Rodrigues, H.; Romao, X.; Andrade-Campos, A.; Varum, H.; Arêde, A.; Costa, A. Simplified hysteretic model for the representation of the biaxial bending response of RC columns. *Eng. Struct.* **2012**, *44*, 146–158. [CrossRef]
13. Yan, C.-w.; Yang, Y.; Jia, J.-q.; Zhang, J.; Liu, S.-g. Study on restoring model of steel reinforced ultra high strength concrete frame joints. *Eng. Mech.* **2015**, *32*, 154–160. (In Chinese)
14. Zhao, G.; Zhang, M.; Li, Y.; Li, D. The hysteresis performance and restoring force model for corroded reinforced concrete frame columns. *J. Eng.* **2016**, *2016*, 7615385. [CrossRef]
15. Guan, D.Z.; Guo, Z.X.; Yang, H.; Yang, S. Restoring Force model of precast beam-column connections incorporating beams with grooves and anchored bottom longitudinal bars. *J. Southeast Univ. Nat. Sci. Ed.* **2018**, *48*, 7. (In Chinese)
16. Sui, Y.; Xue, J.-Y.; Dong, J.-S.; Zhang, X.-C.; Xie, Q.-F.; Bay, F.-Y. The experimental research on the restoring force model of lintel-column joints of concrete archaizing buildings with viscous dampers. *Eng. Mech.* **2019**, *36*, 44–53. (In Chinese)
17. Wei, D.; Suizi, J. Restoring Force Model for Composite-Shear Wall with Concealed Bracings in Steel-Tube Frame. *Buildings* **2022**, *12*, 1315. [CrossRef]
18. Sivaselvan, M.V.; Reinhorn, A.M. Hysteretic Models for Deteriorating Inelastic Structures. *J. Eng. Mech.* **2000**, *126*, 633–640. [CrossRef]
19. Lu, X.; Yin, X.; Jiang, H. Restoring force model for steel reinforced steel-reinforced concrete columns with high steel ratio. *Struct. Concr.* **2013**, *14*, 415–422. [CrossRef]
20. Huan, J.; Guo, X.; Guan, Z.; Yan, T.; Chu, T.; Sun, Z. An Experimental Study of the Hysteresis Model of the Kanchuang Frame Used in Chinese Traditional Timber Buildings of the Qing Dynasty. *Buildings* **2022**, *12*, 887. [CrossRef]
21. Ministry of Construction of the People's Republic of China. *The Standard for Mechanical Properties of Ordinary Concrete: GB/T 50081-2002*; China Construction Industry Press: Beijing, China, 2003.
22. Gao, Y.; Liang, X.; Deng, X. *GB/T 228.1-2010 "Tensile Test for Metallic Materials Part 1: Room Temperature Test Method" Implementation Guide*; China Quality Inspection Press: Beijing, China, 2012.
23. China Academy of Building Science. *The Seismic Test Procedure for Buildings JGJ/T101-2015*; China Construction Industry Press: Beijing, China, 2015.

24. The Society. *Seismic Design Code for Buildings GB50011-2010*; China Construction Industry Press: Beijing, China, 2010.
25. Niu, Z.; Liu, D. Finite element analysis and research of single tunnel double-layer highway tunnel in Loess region. *Highway* **2007**, 221–223. [CrossRef]
26. Pu, W.; Zhang, H.; Xu, X. Simulation of the restoring model of self-centering unbonded prestressed precast concrete frame structure. *Earthq. Resist. Eng. Retrofit.* **2020**, *42*, 8.

Disclaimer/Publisher's Note: The statements, opinions and data contained in all publications are solely those of the individual author(s) and contributor(s) and not of MDPI and/or the editor(s). MDPI and/or the editor(s) disclaim responsibility for any injury to people or property resulting from any ideas, methods, instructions or products referred to in the content.